American Journal of Energy Research, 2024, Vol. 12, No. 3, 55-62
Available online at http://pubs.sciepub.com/ajer/12/3/2
Published by Science and Education Publishing
DOI:10.12691/ajer-12-3-2

Exponential Variation of Irradiance in An Optically Active Water Medium for Potential Applications in Autonomous Underwater System

Raduk Sally Awuor*, Waweru Mugo, Mulati David

Department of Physics, Jomo Kenyatta University of Agriculture and Technology (JKUAT), Nairobi, Kenya
*Corresponding author: sallyraduk2017@gmail.com

Received September 21, 2024; Revised October 23, 2024; Accepted October 30, 2024

Abstract Autonomous underwater vehicles are increasingly used for surface ocean exploration, remote sensing, water-quality monitoring and detailed mapping of ocean floor. These devices typically rely on rechargeable batteries like lithium-ion, and piezoelectric propulsion systems, to provide the electrical energy required to power the vehicles thrust systems. However, some of these devices can incorporate energy harnessing systems such as Photovoltaic (PV) systems, where they can utilize available solar irradiance within the upper layers of the water column, to extend their operational range. In this article, we report on underwater performance of polycrystalline photovoltaic modules under different depths and water conditions. Electrical performance characteristics were analyzed with regard to modified irradiance spectrum traversing water medium. The physical and chemical composition of the water column was investigated and its influence on the decay of irradiance, from white light source, was monitored. A decay in irradiance with depth, from $1000W/m^2$ at air mass $AM1.5$ an irradiance drop to $470W/m^2$ at $0\,cm$ was noted, and continued to decrease to $350W/m^2$ up to a depth of $18cm$. The pH of the water column analyzed was 7.65 and the salinity of the medium was $0.03\,psu$, practical salts units. The measured total dissolved substance in parts per million was 25.6 pp, conductivity in micro Siemens of $51.3\mu S/cm$ of the column solution and resistivity values of $19.3k\Omega.\,cm$ were also recorded. The concentration of salts in the solution was also monitored and the values of potassium and sodium obtained were $2.8\,ppm$ and $12\,ppm$ respectively. A comparative analysis was as well carried out on the percentage loss of irradiance with depth and temperature variations at 12.3°C and 27.7°C. Most amphibious drones designed for shallow depths typically have power wattages ranging from $20W$ to $200W$, and from the irradiance values by plotting the power curves, a maximum power value of $37W$ was obtained.

Keywords: *Underwater, Photovoltaic module, lamp irradiance, Attenuation*

Cite This Article: Raduk Sally Awuor, Waweru Mugo, and Mulati David, "Exponential Variation of Irradiance in An Optically Active Water Medium for Potential Applications in Autonomous Underwater System." *American Journal of Energy Research*, vol. 12, no. 3 (2024): 55-62. doi: 10.12691/ajer-12-3-2.

1. Introduction

One of the rapidly developing technologies in underwater energy generation is use of submerged solar photovoltaic systems [1]. The advancement in technology of submerged solar photovoltaics enables the sustainable appropriate design and delivery of a modern power generating system for marine electronic devices, navigation, defense, and autonomous vehicles, amongst other various applications [1]. The solar spectral distribution changes with water depth, due to attenuation of the radiation traversing a particular medium [2]. The rate of absorption and scattering varies from one material to another; due to the physical properties of the water column like pH, salinity, conductivity, total dissolved substances (TDS) and resistivity [3]. Chemical parameters also affect the amount of radiation observed at a particular depth [4]. At shallow depths, the longer wavelengths ($280-400nm$), like the Ultraviolet spectrum are highly attenuated by the water molecules as well as dissolved organic and suspended matter. The shorter wavelengths (400 700−nm), like the visible spectrum, remain relatively unaffected and penetrate through the water column with minimal attenuation [5,6]. The changes in the solar spectrum as it traverses the water column have important implications for the design and the performance of submerged Photovoltaic systems, as the available solar radiation and its spectral composition can directly impact efficiency and output of these systems [7]. Previous research was carried out on the field experience with performance evaluation of a single-crystalline Photovoltaic panel in an underwater environment. It was discovered that single-crystalline silicon solar cells perform better at shallow depths. At a depth of 5 cm the efficiency recorded was higher, it was found to be 110% as compared to at a depth of $50cm$ which was 80% [8]. The single-crystalline PV panels were further studied in two different on-site locations with various water levels

because the performance of the solar panels is affected by the time of day, solar radiation, and other environmental factors [9]. The underwater spectrum is for that reason biased toward using wider band-gap semiconductors for solar cells ($1.8eV$), thus traditional solar cells that employ narrow-band-gap semiconductors are not optimal for deep-water applications.

1.1. Solar Illumination Underwater

Besides single crystalline silicon cells, a few wide band-gap semiconductors have been investigated for underwater solar cells [10]. It was found that InGaP solar cells with a band-gap of $1.8eV$, could efficiently harness useful solar energy yielding useful power at depths as great as 9 m below the sea level [10,11]. However, the cost of InGaP solar cells has so far been a hindrance in adoption of the technology, though recent advances in the growth of III-V based optoelectronic semiconductors has shown that cost can be greatly reduced [12]. Organic Photovoltaic systems with wide-band gap semiconducting polymers and small molecules have also been investigated [13,14]. These semiconductors have shown to function more efficiently under low-lighting conditions, making them suitable for underwater solar cells applications [15]. Besides the already investigated systems, a large number of organic and inorganic wide-band-gap semiconductors exist that are currently not being considered for solar cell applications due to their band gaps being too large for land-based applications. These types of semiconductors could, however, be highly useful for underwater applications.

2. Methods and Materials

To ascertain transmittance of radiation through the water column, there was a need of determining the physical and chemical properties of the water medium, which contributes greatly to the decay of the radiation. A BT900 Multi-Parameter Meter was used in the Chemistry lab to determine the physical properties of the water sample to be used in studying the traverse of irradiance. Some of the physical parameters under study were; pH, salinity, total dissolved substances (TDS), conductivity and resistivity. This involved inserting each probe of the meter into a beaker containing the fluid sample and each reading recorded. A Flame Photometer FP640 model was used to analyze the chemical properties of that particular water sample under investigation. This entailed measuring the concentration of specific elements in a sample based on the intensity of light emitted when the elements are exposed to a flame.

To obtain standardization calibration using a Flame Photometer, a chronological procedure was followed;

i. Preparing standard solutions: A series of standard solutions with known concentrations of the element sample to be measured were prepared. These concentrations covered the expected range of the concentrations in the sample.
ii. Calibrating the Flame Photometer: The Flame Photometer was calibrated by measuring the emission intensity of the standard solutions. This established a calibration curve relating the intensity of light emitted to the concentration of the element in the sample.
iii. Interpolation concentrations: The calibration curve was used to interpolate the concentrations of the elements in the water sample based on their emission intensities.
iv. Verification and adjustments: Finally, the accuracy of the calibration was verified by measuring the concentration of the water sample and adjusting the calibration curve where necessary.

Results of the Potassium and Sodium concentrations were obtained against emissivity.

A standard testing procedure was followed for testing the performance of a polycrystalline module of $5V$, in relation to irradiance intensity traversing the water column before causing excitation on the cell electrons. The study sought to explore the influence of both water depth and composition on irradiance levels, with a specific focus on assessing the performance of a submerged $5V$ polycrystalline photovoltaic (PV) module. Water depths ranging from 0 to 18 cm were investigated to ascertain their impact. To facilitate controlled depth management of the PV system, a metallic alloy container measuring $29cm*21cm*3cm$, with a thickness of $4.5cm$, was purposefully fabricated as shown in figure 1. These dimensions were selected based on their compatibility with experimental conditions, ensuring optimal performance and reliability throughout the duration of the study.

Water tight insulation was ensured at the junction box and terminals, thus preventing any form of electrolytic corrosion or short circuiting that may occur. The submerged PV module system was illuminated with 37 W lamp at varying depths at intervals of 3 cm. A constant distance of 30 cm was maintained between the water surface and the lamp. The variables recorded were current, voltage and irradiance. The values obtained were dependent on depths. These values were used to determine the I-V characteristics of the submerged modules and its power output while under water.

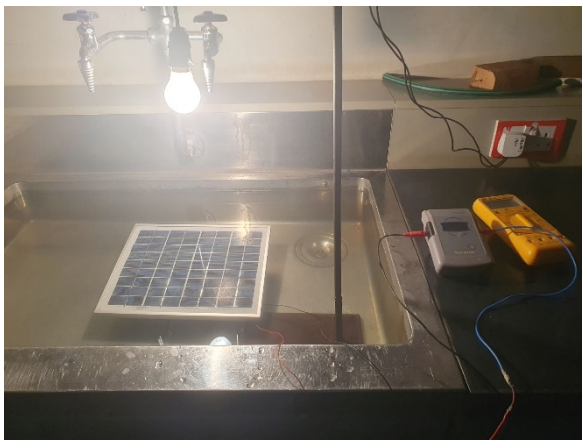

Figure 1. Experimental setup of irradiance investigation with depth

3. Results and Discussion

3.1. Physical and Chemical Composition of the Water Column

The physical and chemical parameters of the water column were studied, as they have direct influence on the transmittance of the radiation through the water column of refractive index, 1.33. The water column temperature was monitored and the obtained value was, 27.7^0C, which was kept constant throughout the experiment. Using a BT900 Multi-Parameter Meter, the pH of the medium was monitored and for this type of medium a value of 7.65 was recorded. The salinity of the medium was also analyzed in terms of practical salt units and a value of 0.03psu salt concentration in that solution was recorded. The value of total dissolved substances (TDS) in parts per million values obtained were 25.6 ppm, conductivity in micro Siemens of 51.3 $\mu S/cm$ of the column solution and resistivity values of 19.3 $k\Omega.\ cm$ were also recorded. These substances are responsible for scattering and absorbing of light intensity across a broad range of wavelengths, affecting the overall attenuation of irradiance in the fluid column.

Flame Spectrometer Model FP640 was used to obtain the chemical parameters of the solution. The nutrients concentration levels in the water also contribute greatly to absorption and scattering of irradiance through the medium. Figure 2 Shows a linear fit of emission intensity against sodium concentration levels in parts per million against emissivity of the standardized calibration.

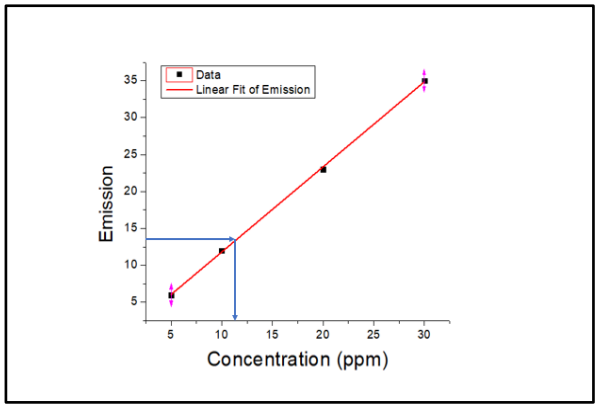

Figure 2. Standardized sodium concentration in the water column

The concentration of Sodium was inferred to be $12\,ppm$ based on the calibration curve established using standard solutions of known sodium concentrations. To obtain the concentration, the emission intensity in counts per second of the sample was compared against the calibration curve established previously with standard solutions of known sodium concentrations.

An intercept value of -0.2712 with a standard error of 0.2861 was obtained. A slope of 1.15 with a standard error of 0.0152 was extracted. This implies that for every $1 ppm$ increase in sodium concentration, the emission increases by 1.15 units. This slope is relatively high, hence consistent increase in emissivity with sodium concentration, though it's less steep than the potassium plot. An adjusted root squared value of 0.9995 was also extracted, this is very close to **1**, this implies an almost perfect fit of the linear model to the data.

Additionally, the amount of Potassium present in the sample was also quantified in terms of concentration in parts per million against emissivity of the standardized calibration of known potassium concentration as shown in Figure 3, a linear fit of emissivity.

The concentration of Potassium in the sample analyzed was inferred to be $2.8 ppm$. The concentration was obtained by comparing the emission intensity in counts per second of the sample solution against the calibrated curve previously established from the standardized solutions of known potassium concentrations.

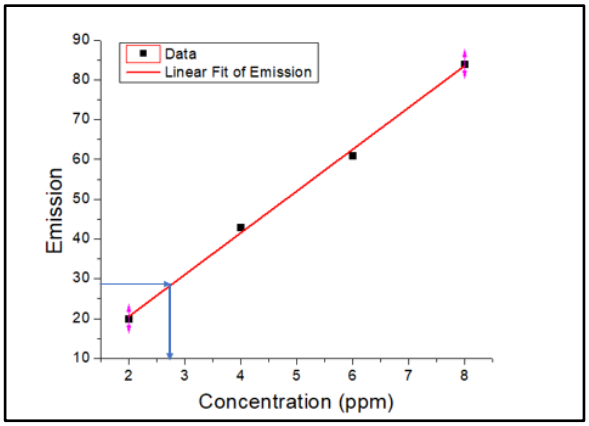

Figure 3. Standardized potassium concentration in the water column

An intercept value of -0.5 with a standard error of 1.936 was obtained. A slope of 10. 5 with a standard error of 0. 3536 was also extracted. This implies that for every 1 ppm increase inpotassium concentration, the emission increases by 10. 5 units. An adjusted root squared value of 0.9966 was also extracted, this is very close to 1, this implies an excellent fit of the linear model to the data and also shows that potassium concentration is the primary factor influencing emissivity.

These linear relationships obtained are very useful as they allow for predictable and consistent traversal of irradiance through the medium to the target PV module. These observed slope values are considered to be relatively low, thus suggesting a more stable and predictable relationship between the measured emissions against potassium and sodium concentration, hence, the performance and reliability of submerged PV can as well be predicted. Both the physical and chemical parameters actively contributed to absorption, scattering, reflection, transmission, attenuation and density of the fluid. They directly determine the amount of light intensity available in the fluid column [16].

3.2. PV Module Power Output As A Function of the Operating Temperature with Regards to the Submersion Depth

The analysis of power output for a submerged photovoltaic (PV) module at different water temperatures and depths, as illustrated in the graphs; Figure 4 (a) PV module power output at 12.3^0C and Figure 4 (b) PV module output at 27.7^0C, provides important insights for understanding the thermal effects on PV system performance. In both figures, power against depth curves were obtained based on the data points exhibiting polynomial fittings, because the relationship between the

variables is non-linear. As solar PV depth increases, the radiation encounters a greater path length through the water column. This results in two phenomena, absorption and scattering, that affect the electrical output of the module [17]. This type of analysis is valuable for applications of submerged PV for autonomous systems.

In Figure 4 (a), at a medium temperature of 12. 3°C, the power output starts high at 37 W at the surface, 0 cm depth, and decreases with increasing depth. At 5 cm, the power output is 30 W, while at, it drops to 25 W. By the time the depth reaches 18 cm, the power output is approximately 15 W.

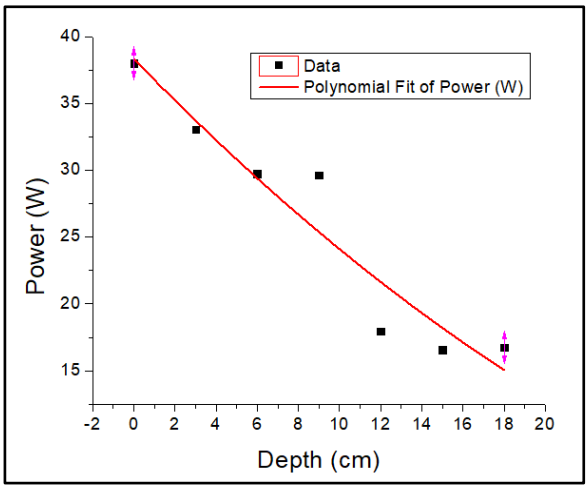

Figure 4. (a) PV module power output at 12.3°C

Adjusted root square of 0.8767 was obtained. This indicates that 87.7% of the variability in power output can be explained by the polynomial model which adequately represents the power-depth relationship at 12.3°C. An intercept value of 38.3169 W was obtained, this indicates the power output of our module at the water surface, that is at 0cm depth. This obtained value suggests that the module obtains higher power output when exposed at the surface, which is consistent while water is at a cooler temperature (12.3°C), thus effectively managing the module's thermal drift and enhancing its efficiency.

For the first order coefficient, B1, a negative value of − 1. 5838 was obtained with a standard error of ± 0. 6984, the value indicates that the power output decreases linearly with depth. For each centimeter increase in depth, the power output drops by approximately 1. 58 W. The cooling effect at 12. 3°C leads to improved module efficiency, but with decrease in solar radiation as depth increases due to the absorption, scattering, angle of incidence, wavelength dependence and density variation, attributed to its composition [18,19]. Cooler water is denser, which leads to greater scattering of light. More particles and molecules in a given volume cause light to scatter or absorb more, thus reducing the depth to which irradiance can penetrate. The second order coefficient, B2, has a small positive of 0. 0162. This suggests that the rate of power decrease slows down slightly at greater depths.

In Figure 4 (b), at a water temperature of 27.7°C, the power output also starts at 37W at the surface but declines more rapidly with depth. By 5cm depth, the output is 35W , and at 10cm , it drops sharply to 20W . At depths of 15cm and beyond, the power output reduces to below 10W .

An adjusted root square of 0.9608 was obtained. This indicates that 96.1% of the variability in power output can be explained by the polynomial model, this shows a better fit compared with 12.3°C. An intercept value of 42.7W was obtained, this initial power output at the warmer water surface (27.7°C) is higher as compared to the value at cooler temperatures of 12.3°C. For the warmer water, a larger standard error of ± 5. 9310 W was obtained in the intercept, this is attributed by low density of the medium indicating more variability compared to cooler water which was ± 2. 6841 W.

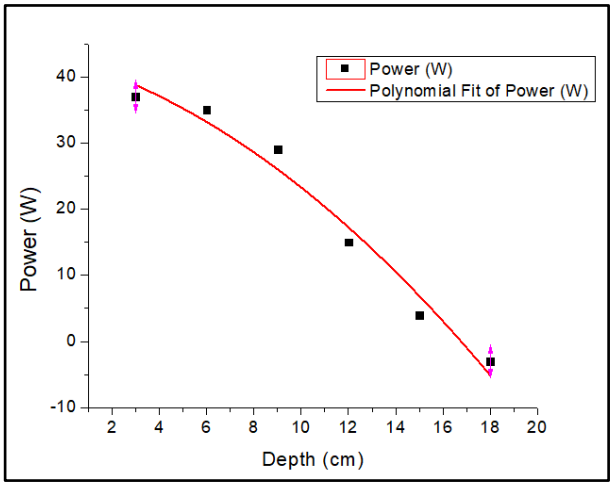

Figure 4. (b) Power generated against Solar PV depth at 27.7°C

A first order coefficient, B1, negative value of -1.0488 was obtained, it shows the rate of power decrease with depth, however, it is lower than the rate of decrease at cooler water. For each increase in depth, the power dropped with 1.05W . Despite the lower rate of power decrease, the larger standard error in the B1, 1.2934, in the warmer water poses uncertainty to the model. The negative second-order coefficient, B2, − 0. 0893 indicates downward curvature in the power depth relationship. This implies that the rate of power loss accelerates with increasing depth due to absorption of the infrared spectrum at the shallow depth. The small value of B2 suggests a modest effect, but the downward curvature contrasts with the slight upward curvature seen at 12.3°C

The warmer water temperature (27.7°C) reduces the module's efficiency more significantly due to less effective heat dissipation. This can be attributed to the fact that higher temperatures increase the resistance within the PV cells, thus reducing their power output [20,21].

Additionally, the warmer water does not provide sufficient cooling to mitigate the heat generated by the module. The power decline is steeper at 27.7°C than at 12.3°C, indicating a more significant loss of efficiency due to higher temperatures. This behavior reflects the general observation that PV modules lose efficiency as temperatures rise beyond their optimal operating range [22,23].

3.3. PV Module Power Density As A Function of the Operating Temperature with Regards to Submersion Depth

Similarly, the analysis of a linear regression of power density for a submerged photovoltaic (PV) module at different water temperatures and depths, as illustrated in the graphs; Figure 5 (a) Irradiance (W/m^2) against PV module depth at 12.3°C and Figure 5 (b) Irradiance (W/m^2) against PV module depth at 27.7°C, provides important insights for understanding the thermal effects on PV system performance. The irradiance represents the amount of solar radiation reaching the PV module, which impacts the power density output.

In Figure 5(a), the curve of irradiance against PV module depth, it was observed that maximum irradiance, $410W/m^2$, could be obtained at the surface, $0cm$ depth, this was also shown by an intercept value obtained of $409.57W/m^2$. This value of irradiance decreased steadily as depth increased. At a depth of $18cm$, the irradiance value had decreased to $360W/m^2$. A negative slope value of $-2.7619\frac{W}{m^2}/cm$, was obtained. This implies that for every centimeter depth increase, the irradiance decreases by $2.7619W/m^2$. The negative slope suggests a steady decline in irradiance with depth, as the water column attenuates the incident irradiance, which becomes more significant with depth [23].

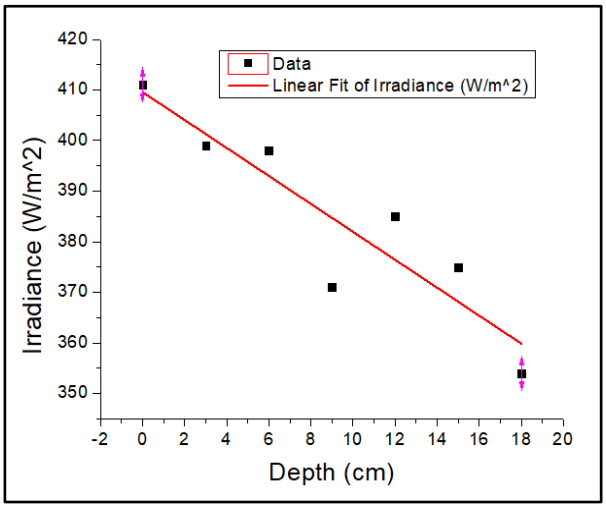

Figure 5. (a) Irradiance against depth at 12.3°C

An adjusted root square value of 0.80405 was obtained. This denotes that 80.4% of the variability in irradiance can be explained by the depth of submersion at this temperature, 12.3°C. This correlation implies that submersion depth has a direct influence on the irradiance value obtained at a depth. Despite the decay in irradiance with depth, a smaller slope in cooler temperatures implies that the rate is not as steep as in warmer water conditions. This reveals that the submerged PV module will receive more irradiance and have better performance, higher power density, at this temperature as compared to higher temperatures.

To quantify the attenuation of irradiance at each temperature, we can calculate the percentage of irradiance lost using equation 1 [24].

$$Percentage\ loss = \left(1 - \frac{I(d)}{I_o}\right)100 \qquad (1)$$

Where $I(d)$ is the irradiance at depth d and I_o is the initial irradiance at the surface.

This equation expresses the fraction of light lost as a percentage of the initial irradiance. It accounts for the decrease in light intensity as it travels through the water column, considering both absorption and scattering effects. The result provides a measure of the optical attenuation in the medium, which can vary with temperature due to changes in water intermolecular and potentially dissolved constituents.

By applying this formula at various depths and temperatures, we can quantitatively compare the light attenuation characteristics under different conditions, offering insights into the optical properties of the water at each temperature. To obtain the percentage of irradiance attenuated at 12.3°C: Initial irradiance at $0cm$ is $410W/m^2$, final irradiance at $18cm$ is $355W/m^2$.

To obtain the percentage of irradiance lossed;

$$\left(1 - \frac{355}{410}\right)100 = 13.41\%$$

This implies that 13.41% of the irradiance was lossed overally in the medium between 0 cm depth to $18cm$ depth.

In Figure 5 (b), the curve of Irradiance against PV module depth at 27. 7°C, it was observed that maximum irradiance of 450 W/m^2, could be obtained at the surface, 0 cm depth, and it decreased sharply with an increase in depth. At a depth of 18 cm the irradiance value drops to 370 W. A steep slope of − 6. 7619 $W/m^2/cm$ was obtained, steeper than at 12. 3°C, showing a faster rate of irradiance loss as depth increases. This suggests that, for every centimeter of depth, irradiance decreases by 6. 7619 W/m^2, proving that light is more attenuated at high temperatures. The reduction in irradiance is attributed to the difference in light refraction between water at 27.7°C and 12.3°C. The warmer water (27.7°C) has a lower refractive index, causing light to bend less sharply as it passes through. Conversely, the cooler water (12.3°C) has a higher refractive index, resulting in a sharper bending of light. This difference in refraction contributes to the observed loss of irradiance [25].

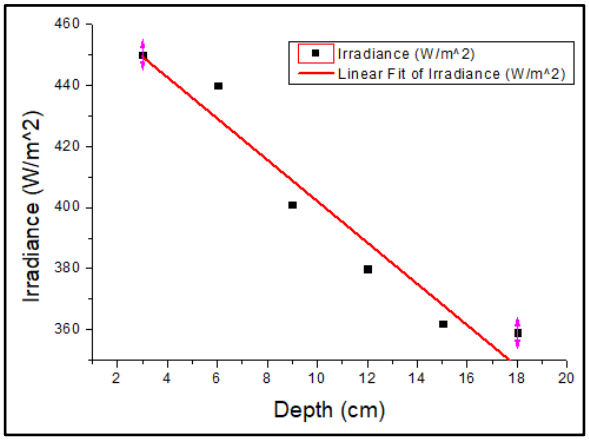

Figure 5. (b) Irradiance against PV module depth at 27.7°C

An adjusted root squared value of 0.93206 was obtained. This value suggests a very strong correlation between depth

and irradiance, with 93.2% of the irradiance being accounted for by the depth. This directly affects the output of the module as shown by the Figure (b) above.

At 3 cm depth, an irradiance value of 450 W/m^2 was recorded, at 18 cm depth, the irradiance had dropped to 360 W/m^2.

The percentage loss of irradiance between 3 cm to 18 cm depth was found to be;

$$\left(1-\frac{360}{450}\right)100 = 20\%$$

These linear fits showing a relationship of irradiance and submerged PV modules depths, provides a mathematical model that can be used to predict the irradiance levels at different depths. Thus, enabling more accurate design and optimization of submerged PV modules with potential applications in amphibious drones. The gradual decay of irradiance with depth can be attributed to the cumulative effects of Inherent Optical Properties of the water column like, absorption coefficient, scattering coefficient and the volume coefficient [26,27]. The specific concentrations of sodium, potassium and other dissolved substances along with pH and salinity influences the optical properties of the water and contribute to the observed attenuation patterns.

The decrease in irradiance with depth has a direct consequence with the electrical output of our modules, in that; there is a decrease in the overall current generated by the panel as the number of photons absorbed by the solar cells and converted into electricity reduces as irradiance weakens, and in some cases decrease in irradiance can initially lead to a slight increase in voltage output. This is because weaker radiation is just sufficient to improve the efficiency of certain solar cell materials under specific conditions [28]. This has a significant implication for various underwater applications. Understanding light attenuation is essential for underwater optics activities like underwater photography, videography, imaging and remote sensing techniques that rely on accurate light measurement [29].

Besides, this knowledge is important in designing efficient underwater solar cells. Tailoring the materials to be more sensitive to wavelengths that penetrate deeper in water can improve their efficiency in low-light underwater environments. An investigation is made on the performance of the visible light communication systems when exposed to ambient noise. Although the absolute intensity of the solar radiation is lower underwater, the spectral content is narrow and thus lends itself to high conversion efficiency if a solar cell is well matched to the wavelength range [30].

The attenuation of light in water exhibits a clear wavelength dependence. Longer wavelengths in the red and orange portions of the visible spectrum experience the most rapid attenuation, particularly near the water's surface. This is followed by intermediate attenuation rates for yellow and green wavelengths. In contrast, shorter wavelengths - blue, indigo, and violet - demonstrate the least attenuation, allowing them to penetrate deeper into the water column.

This wavelength-dependent attenuation phenomenon aligns with established optical principles in aquatic environments. The differential absorption and scattering of light based on wavelength contribute to the characteristic color and transparency properties of water bodies at varying depths. This pattern of attenuation has significant implications for underwater light availability, affecting processes such as the design of underwater optical systems.

It's worth noting that while the general trend described here is consistent with accepted scientific understanding, the specific attenuation rates can vary depending on factors such as water chemical composition, suspended particles, and dissolved organic matter. Additionally, temperature also influence these optical properties, as suggested by the comparison between 12.3°C and 27.7°C conditions. Thus, from our analysis we can deduce that irradiance obtained within the medium is directly proportional to depth as expressed by the following expression;

$$I_o = 100\%\ of\ \ the\ incident\ irradiance$$
$$I = 80\%I_o$$

therefore; Transmittance, $T = \frac{I}{I_o} = 80\%$

$$= \left[100\%\left(300-450nm\right)\right]$$

That is for 27.7°C, being that 20% of the incident irradiance was lossed through the column and the remaining 80% is expressed as a whole fraction of the blue spectrum ($300-450\,nm$), which was least attenuated. For the water column at 12.3°C where the percentage in the column obtained was 13.4% , the expression would be;

$$I_o = 100\%\ of\ \ the\ incident\ irradiance$$
$$I = 86.6\%I_o$$

therefore; Transmittance, $T = \frac{I}{I_o} = 86.6\%$

$$= \left[100\%\left(300-450nm\right)\right]$$

This deduction can be compared to a study carried out on the apparent optical properties of the sea - observation overview and water column relationships. The measured and modeled depths of the 1% and 10% light levels are compared for different wavelengths. For both the light levels, the model predicted higher value of 300-450 nm spectrum in the measured depth of the 10% light level as compared to the measured depth of the 1% light levels [31].

3.4. Comparative Analysis On the Influence of Temperature on Irradiance Propagation Across Water Column With Regards to Application of Submerged PV Module

Similarly, a comparative analysis was carried out on the transmittance of irradiance with depth between the two temperatures, at 12.3°C and 27.7°C as shown in Figure 6. It was observed that at both the temperatures, the curves

depicted a decrease in irradiance with an increase in depth trends. A polynomial model was applied to fit the irradiance values at each depth, yielding insights into how temperature influences irradiance decay. The analysis considered the adjusted R-squared values to evaluate the model's accuracy at each temperature. The results indicate a distinct variance in irradiance attenuation profiles between the two temperatures. At 27.7°C, irradiance exhibited a steeper decrease with depth compared to measurements taken at 12.3°C. This observation is evidenced by both the polynomial fits and the calculated parameters.

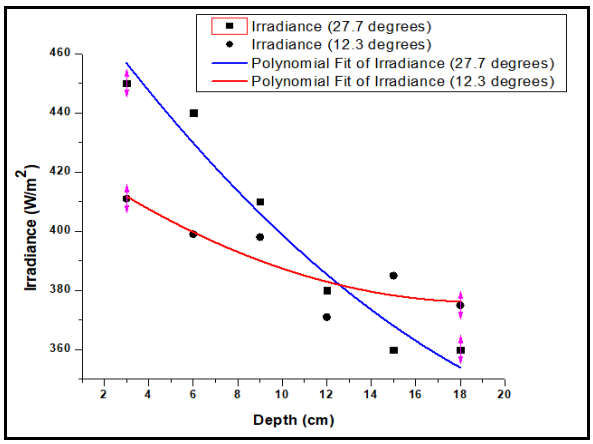

Figure 6. Comparison of Irradiance against depth at 12.2°C and 27.7°C

At the column temperature of 27.7°C, an intercept value of 487 was recorded while at 12.3°C it was found to be 424, this signifies that the initial irradiance was higher at 27.7°C. This can be attributed to increased molecular activity at elevated temperatures, allowing more radiant energy to be absorbed initially.

The coefficients B1 and B2 in the polynomial model reflect the irradiance decay rate. For 27.7°C, the first order coefficient, B1, is -10.2074 and the second order coefficient, B2, is 0.7857, indicating a rapid decline in irradiance as depth increases. Conversely, at 12.3°C, B1 and B2 values of -5.2841 and 0.1388 respectively signify a more gradual decline.

The adjusted R-squared values, 0.9836 for 27.7°C and 0.6148 for 12.3°C, suggest that the polynomial model describes the irradiance attenuation more accurately at higher temperatures. The reduced fit at 12.3°C may imply temperature-dependent variations in the material's structure or composition, affecting irradiance consistency.

The observed disparity in irradiance attenuation rates at different temperatures can be attributed to thermally induced changes in the water column, which alters its intermolecular structure. This infers that in the warmer column, 27.7°C, the molecules exhibit increased kinetic energy, resulting in higher vibrational and translational motion, which leads to enhanced scattering or absorption of radiant energy, thereby accelerating irradiance decay with depth. Conversely, in the cooler water column, molecular motion is relatively reduced, with molecules maintaining closer proximity to each other, this may allow irradiance to penetrate more deeply with less dispersion [32].

The combination of these molecular-level effects contributes to the observed differences in irradiance values at various temperatures and depths. The absorption and scattering rates of different wavelengths within the light spectrum are influenced by these temperature-dependent molecular properties.

4. Conclusion

The PV systems have been found out to work well in submerged conditions. The experimental study of submerged polycrystalline PV systems in shallow and moderate water depths was investigated under a lab setup. This study has provided a preliminary understanding of the performance behavior of underwater photovoltaics. Based on the experimental results, it is understood that the output power is less in deep waters, hence the use of underwater photovoltaic systems can be encouraged for low power applications, under controlled depths.

Additionally, irradiance obtained within the water column is directly proportional to depth and temperature of the column. The data reveal a marked difference in irradiance attenuation profiles, suggesting that temperature significantly impacts energy dispersion within the material. This study confirms that temperature exerts a substantial influence on irradiance propagation through materials, with higher temperatures accelerating the rate of irradiance attenuation.

References

[1] Enaganti, P. K., Soman, S., Devan, S. S., Pradhan, S. C., Srivastava, A. K., Pearce, J. M., & Goel, S. "Dye - sensitized solar cells as promising candidates for underwater photovoltaic applications". Progress in Photovoltaics: Research and Applications, vol. 30, no. 6, p. 632-639, 2022.

[2] Fischer, R., Ting, A., DiComo, G., Prosser, J., Peñano, J., Hafizi, B., & Sprangle, P. "Absorption and Scattering of 1.06 μm laser radiation from Oceanic aerosols". Applied optics, vol. 48, no. 36, p. 6990-6999, 2009.

[3] Reul, N., Fournier, S., Boutin, J., Hernandez, O., Maes, C., Chapron, B., ... & Delwart, S. "Sea surface salinity observations from space with the SMOS satellite: A new means to monitor the marine branch of the water cycle". Surveys in Geophysics, vol. 35, p. 681-722, 2014.

[4] Williamson, C. E., Overholt, E. P., Brentrup, J. A., Pilla, R. M., Leach, T. H., Schladow, S. G., ... & Neale, P. J. "Sentinel responses to droughts, wildfires, and floods: effects of UV radiation on lakes and their ecosystem services". Frontiers in Ecology and the Environment, vol. 14, no.2, p. 102-109, 2016.

[5] J. A. Muaddi and M. A. Jamal. "Solar spectrum at depth in water." Renewable Energy, vol. 1, p. 31, 1991.

[6] M. A. Jamal and J. A. Muaddi, "Solar energy at various depths below a water surface." J. Energy Res., vol. 14, p. 859, 1990.

[7] J. A. Muaddi and M. A. Jamal, "Spectral response and efficiency of a silicon solar cell below the water surface." Sol. Energy, vol. 49, p. 29, 1992.

[8] Rosa-Clot, M., Rosa-Clot, P., Tina, G. M., & Scandura, P. F. "Submerged photovoltaic solar panel: SP2. Renewable Energy", vol. 35, no. 8, p. 1862-1865, 2010.

[9] M. Rosa-clot, P. Rosa-clot, R. Lanzafame, S. Nachtmann, M. Rosa-clot, P. Rosa-clot, P. F. Scandura, S. Taddei, and G. M. Tina, "Field experience with performance evaluation of a Single-crystalline photovoltaic panel in an underwater environment." IEEE Transactions on Industrial Electronics, vol. 57, p. 2492, 2010.

[10] Jenkins, P. P., Messenger, S., Trautz, K. M., Maximenko, S. I., Goldstein, D., Scheiman, D., ... & Walters, R. J. "High-bandgap solar cells for underwater photovoltaic applications". IEEE Journal of Photovoltaics, vol.4, no.1,p. 202-207, 2013

[11] Notman, N. "Underwater solar cells". Materials Today, vol. 7 no. 15, p. 301, 2012.

[12] Simon, J., Schulte, K.L., Horowitz, K.A.W., Remo, T., Young, D.L., and Ptak, A.J. “III- V-based optoelectronics with low-cost dynamic hydride vapor phase epitaxy”. Crystals, vol. 9, p. 1–14, 2019.

[13] Walters, R.J., Yoon, W., Placencia, D., Scheiman, D., Lumb, M.P., Strang, A., Stavrinou, P.N., and Jenkins, P.P. “Multijunction organic photovoltaic cells for underwater solar”. IEEE 42nd Photovoltaic Specialist Conference (PVSC), p. 1–3, 2015.

[14] Kong, J., Nordlund, D., Jin, J.S., Kim, S.Y., Jin, S.-M., Huang, D., Zheng, Y., Karpovich, C., Sertic, G., Wang, H., et al. “Underwater organic solar cells via selective removal of electron acceptors near the top electrode”. ACS Energy Lett, vol. 4, p. 1034–1041, 2019.

[15] Steim, R., Ameri, T., Schilinsky, P., Waldauf, C., Dennler, G., Scharber, M.,and Brabec, C.J. “Organic photovoltaics for low light applications”. Sol. Energy Mater. Sol. Cells, vol. 95, p. 3256–3261, 2011.

[16] Dera, J., & Wozniak, B. “Solar radiation in the Baltic Sea. Oceanology”, vol. 52, no. 4), 2010.

[17] Jonasz, M., & Fournier, G. “Light scattering by particles in water: Theoretical and experimental foundations”. Elsevier. 2010.

[18] Reul, N., Fournier, S., Boutin, J., Hernandez, O., Maes, C., Chapron, B., ... & Delwart, S. “Sea surface salinity observations from space with the SMOS satellite: A new means to monitor the marine branch of the water cycle”. Surveys in Geophysics, vol. 35, p. 681-722, 2014.

[19] Williamson, C. E., Overholt, E. P., Brentrup, J. A., Pilla, R. M., Leach, T. H., Schladow, S. G., ... & Neale, P. J. “Sentinel responses to droughts, wildfires, and floods: effects of UV radiation on lakes and their ecosystem services”. Frontiers in Ecology and the Environment, vol. no.2, p. 102-109, 2016.

[20] Bensalem, S., Chegaar, M., Herguth, A.,. “Band gap dependence with temperature of semiconductors from solar cells electrical parameters”. Curr. Appl. Phys. vol. 17, p. 55–59, 2017.

[21] Geng, P., Li, W., Zhang, X., Zhang, X., Deng, Y., Kou, H., . “A novel theoretical model for the temperature dependence of band gap energy in semiconductors”. J. Phys. D: Appl. Phys. p. 50, 2017.

[22] Fébba, D. M., Rubinger, R. M., Oliveira, A. F., & Bortoni, E. C.. “Impacts of temperature and irradiance on polycrystalline silicon solar cells parameters”. Solar Energy, vol. 174, p. 628-639, 2018.

[23] Berthod, C., Strandberg, R., Yordanov, G.H., Beyer, H.G., Odden, J.O.,. “On the variability of the temperature coefficients of mc-si solar cells with irradiance”. Energy Procedia vol. 92, p. 2–9, 2016.

[24] Skirtach, A. G., Karageorgiev, P., De Geest, B. G., Pazos‐Perez, N., Braun, D., & Sukhorukov, G. B. “Nanorods as wavelength‐selective absorption centers in the visible and near‐infrared regions of the electromagnetic spectrum”. Advanced Materials, vol. 20, no. 3, p. 506-510, 2008.

[25] Downing, B. D., Pellerin, B. A., Bergamaschi, B. A., Saraceno, J. F., & Kraus, T. E. “Seeing the light: The effects of particles, dissolved materials, and temperature on in situ measurements of DOM fluorescence in rivers and streams”. Limnology and Oceanography: Methods, vol. 10, no. 10, p. 767-775, 2012.

[26] Wang, G., Cao, W., Yang, D., & Xu, D. “Variation in down welling diffuse attenuation coefficient in the northern South China Sea”. Chinese Journal of Oceanology and Limnology, vol. 26, p. 323-333, 2008.

[27] Wang, M., Son, S., & Harding Jr, L. W. Retrieval of diffuse attenuation coefficient in the Chesapeake Bay and turbid ocean regions for satellite ocean color applications. Journal of Geophysical Research: Oceans, p. 114(C10), 2009.

[28] Green, M. A. Third generation photovoltaics: solar cells for 2020 and beyond. Physical E: Low-dimensional Systems and Nanostructures, vol. 14, no. 1-2, p. 65-70, 2002.

[29] Dolin, L. S., & Levin, I. M. Underwater optics. Digital Encyclopedia of Applied Physics. 2003.

[30] Schubert, J., Oliva, E., Dimroth, F., Guter, W., Loeckenhoff, R., & Bett, A. W. High-voltage GaAs photovoltaic laser power converters. IEEE Transactions on Electron Devices, vol. 56 no. 2, p. 170-175, 2009.

[31] Antoine, D., Hooker, S. B., Bélanger, S., Matsuoka, A., & Babin, M. “Apparent optical properties of the Canadian Beaufort Sea–Part 1: Observational overview and water column relationships”. Biogeosciences, vol. 10, no. 7. p. 4493-4509, 2013.

[32] Katsukura, H., Miyata, T., Shirai, M., Matsumoto, H., & Mizoguchi, T. “Estimation of the molecular vibration of gasses using electron microscopy”. Scientific Reports, vol. 7, no. 1, p. 16434, 2017.